Indian Journal of Engineering & Materials Sciences
Vol. 29, October 2022, pp. 586-593
DOI: 10.56042/ijems.v29i5.46815

Hydrothermal Synthesis of Rare Earth Co-Doped Cerium Oxide: Influence on Phase Composition, Characterization, and Photocatalytic Activity

Handan ÖZLÜ TORUN[a]*, & Rabia KIRKGEÇİT[b]

[a]Department of Energy Systems Engineering, Elbistan Faculty of Engineering, Kahramanmaraş İstiklal University, Kahramanmaraş 46 300, Turkey

[b]Material Science and Engineering, Institute of Science, Kahramanmaraş Sütçü İmam University, Kahramanmaraş 46 050, Turkey

Received: 24 February 2021; Accepted: 21 September 2021

In this study, the synergistic effect of CeO_2-based ternary photocatalytic behavior was investigated. The rare earth element pair was doped to improve CeO_2 photocatalytic performance. Cerium oxide (CeO_2) and co-doped $Ce_{0.85}La_{0.10}M_{0.05}O_2$; *M*: (Sm, Gd, Dy, Er, Ho, Y) were prepared using the hydrothermal method. The synthesized compounds were examined with various analysis techniques. It was determined that the unit cell parameter varied according to the average diameters of the additive types. The relationship between the crystal parameter and degradation was examined. It was also determined that the particle size of the compounds changed in nm sizes. The Tauc plot was used in the calculation of the band range. The lowest band range 2.02 eV was observed in the $Ce_{0.85}La_{0.10}Gd_{0.05}O_2$ compound. The cationic dyestuff methylene blue was used in the catalytic experiments. The behavior of the compound with the dyestuff was also examined and a xenon lamp was used in order to observe the particle effect. When the results of the catalytic experiments were evaluated, it was shown that the added particles disintegrated the dyestuff and that the methylene blue degradation of the $Ce_{0.85}La_{0.10}Gd_{0.05}O_2$ compound was 71% (at 120 min).

Keywords: CeO_2, Hydrothermal, Trivalent ion doping, Methylene blue, Photocatalysis degradation

1 Introduction

Advances in the textile industry and the use of different dyes currently pose an environmental threat. The release of dyes into wastewater without degradation pollutes the water and soil. One of the best ways to prevent contamination is to remove organic dyes using photocatalytic reduction[1, 2]. The photocatalytic mechanism can be explained as follows. Ultraviolet (UV) lights stimulate electron and hole pairs. Photo-electrons react with O_2 to form O_{2-} anion radicals. The holes react with water to analyze active OH radicals. These active species are fragments of organic dye compounds[3]. Necessary factors for an ideal photocatalyst include: i) high chemical stability, ii) low cost, iii) non-toxicity, and iv) high photocatalytic activity[4]. Cerium oxide (CeO_2) and its compounds are quite noteworthy and possess these properties. Moreover, CeO_2, which is in the semiconductor class, has many applications. For example, Lahitha et al[5]. researched the effect of CeO_2 on degradation in textile dyes. Ying Xue et al[6]. used CeO_2 nanoparticles as an antioxidant in biomedical treatments. Zhijie Li et al[7]. employed the gas sensor application of CeO_2 nanoparticles synthesized using the hydrothermal method. Zhang et al[8]. researched the oxygen storage features of CeO_2 nanocubes. Karran Woan et al[9]. investigated the photoluminescence features of the CeO_2 compound. Abdullah et al[10]. used CeO_2 as an electrolyte in a solid oxide fuel cell application.

In wastewater management and disposal of organic pollutants, the CeO_2 compound absorbs and releases oxygen ions during the Ce^{3+} / Ce^{4+} cycle[11]. However, the pure CeO_2 semiconductor band gap is 3.2 eV[12]. This situation restricts working in the visible region. Metal or nonmetal elements are added to the CeO_2 structure to reduce the band gap. Until now, the photocatalytic properties of different species have been investigated by augmenting the CeO_2 compound. The addition of metal ions to the CeO_2 semiconductor may cause a decrease in thermodynamic stability and separation of the e^- / h^+ pair during photocatalysis [13]. In order to eliminate this negativity, rare earth elements and nonmetal elements have become quite remarkable as additives. The activities of photocatalysts are related to the radius of the doping ion and the doping method[14,15,16]. In this study, different rare earth elements on the photocatalytic

*Corresponding author (E-mail:handan.ozlutorun@istiklal.edu.tr)

behavior of CeO_2 was investigated for structure stability. Different rare earth element pairs were doped to the CeO_2 structure with the co-doping method, which is frequently used in crystal structure improvements. As rare earth elements, Gd, Sm, La, Dy, Er, and Y were selected, and syntheses were performed via the hydrothermal method. Methylene blue was used to investigate the photocatalysis behavior of the compounds obtained. The research results were compared according to the crystal structure changes.

2 Material and Methods

Pure CeO_2 and co-doped CeO_2 compounds were synthesized using the hydrothermal method. In the co-doping study, the formulation was determined as $Ce_{0.85}La_{0.10}M_{0.05}O_2$ (gadolinium /Gd, samarium/Sm, holmium/Ho, lanthanum/La, erbium/ Er, dysprosium/ Dy, and yttrium /Y). As starting compounds, the synthesis reactions used: $Ce(NO_3)_3 6H_2O$, $La(NO_3)_3 6H_2O$, $Sm(NO_3)_3 6H_2O$, $Gd(NO_3)_3 6H_2O$, $Ho(NO_3)_3 5H_2O$, $Dy(NO_3)_3 5H_2O$, $Er(NO_3)_3 6H_2O$, and $Y(NO_3)_3 6H_2O$. After stoichiometric weighing, the compounds to be obtained according to the formula ($Ce_{0.85}La_{0.10}M_{0.05}O_2$) were dissolved in distilled water. Next, 6 M NaOH was added dropwise into the solution and it was then stirred for 30 min. The obtained mixture was placed in a Teflon-coated steel autoclave and heat treatment applied for 18 h at 180 °C. Following the heat treatment, the solution was dried and washed with distilled water several times. After the washing process, the samples were sintered for 12 h at 800 °C.

All obtained compounds were subjected to characterization analyses. Crystal structure was examined via X-ray diffraction (XRD; Philips X 'Pert Pro, λ = 0.154056 nm, Cu-Kα radiation). Chemical structural analysis was carried out at a wavelength of 785 nm and examined using 30 mW diode laser Raman spectroscope with a resolution of 3 cm^{-1}. The Zeiss EVO 10LS scanning electron microscope (SEM-EDS) was used in the microstructural and elemental analyses of the samples. Photocatalytic behavior was investigated via UV spectroscopy (UV-1800 Shijadzu UV spectrophotometer).

The photocatalytic activities of the pure and doped CeO_2 samples were examined using a 300 W xenon lamp in the visible wavelength range. Methylene blue was used as the dyestuff. The solution was prepared as a 5 ppm dyestuff concentration. Measurements were taken using 30 mg of particles as the amount of photocatalyst. For each measurement, a 2-mL sample solution was used. The effect of the solar simulator used without particles on the dyestuff was also examined. Before the measurements, the particle-augmented dyestuff solution was kept 30 min in a dark environment. The mixing process of the solution continued under the xenon lamp throughout the measurement. The measurements were performed at different periods, starting from the 0th min to the 100th min.

3 Results and Discussion

The crystals of pure CeO_2 and $Ce_{0.85}La_{0.10}M_{0.05}O_2$ (Gd, Sm, Ho, La, Er, Dy, and Y) compounds exhibited a cubic fluorite structure. Figure 1 shows the X-ray diffraction structures of all the samples. No impurity peaks were seen at the selected sintering temperature. The added rare earth elements formed a cubic crystal lattice and the crystal structure was preserved, as shown in Fig. 2[17]. The insertion of the rare earth element into the crystal lattice via doping can be observed. This situation is explained in the following paragraph.

In the main structure of CeO_2, Ce^{4+} ions are located superficially at the corners, while oxygen ions are

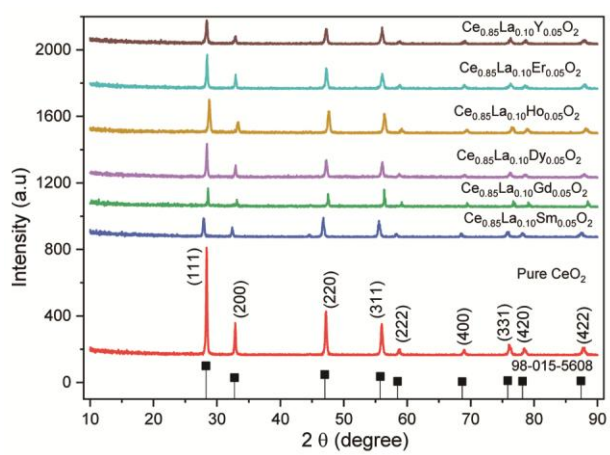

Fig. 1 — XRD patterns of pure and doped CeO_2 powder samples: (a) pure CeO_2, (b) La, Sm co-doped CeO_2, (c) La,Gd co-doped CeO_2, (d) La,Dy co-doped CeO_2, (e) La,Ho co-doped CeO_2, (f) La,Er co-doped CeO_2, and (g) La,Y co-doped CeO_2.

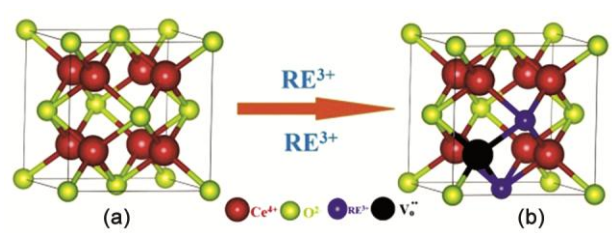

Fig. 2 — a) Crystal structure of CeO_2, and b) Crystal structure of doped CeO_2.

Table 1 — XRD analysis contents of pure and co-doped CeO_2 powders

Samples	Lattice parameters	Space Group	Volume	Crystalline size (nm)				Micro strain (%)			
	a (Å)		(Å)^3	Mean value	(111)	(220)	(311)	Mean value	(111)	(220)	(311)
Pure CeO_2	5.4127	Fm-3m	158.58	53.77	76.48	26.84	27.99	0.31	0.23	0.36	0.29
CeLaDy	5.4450	Fm-3m	161.39	48.19	76.45	22.17	27.95	0.27	0.20	0.44	0.29
CeLaEr	5.4411	Fm-3m	161.10	38.29	55.98	26.81	23.09	0.29	0.28	0.35	0.36
CeLaY	5.4452	Fm-3m	161.40	28.36	32.17	26.82	23.08	0.41	0.48	0.35	0.36
CeLaGd	5.4724	Fm-3m	163.86	28.59	32.15	11.86	26.76	0.55	0.49	0.85	0.36
CeLaSm	5.4481	Fm-3m	161.76	41.31	55.98	34.02	27.93	0.28	0.28	0.28	0.29
CeLaHo	5.4203	Fm-3m	159.22	24.87	25.36	22.22	27.98	0.57	0.61	0.42	0.29

located in the tetrahedral spaces of the cubic unit cell. All Ce^{4+} ions are located in the 4a region, which has an atomic coordinate (000). Oxygen ions are located in the 8c region and have atomic coordinates (1 / 4.1 / 4.1 / 4). When different elements are added to the fluorite-structured CeO_2, the Ce atom is replaced with this doped element, and oxygen ion spaces are formed. As a result of this displacement in the crystal lattice, the unit cell parameter and crystal sizes vary. Using the XRD analysis, the crystal sizes of all samples were calculated according to the Debye-Scherrer equation. The resulting crystal sizes of 111, 220, and 311 planes calculated using the Debye-Scherrer equation are summarized in Table 1. Nano-sized crystal structures were obtained via hydrothermal synthesis. The crystal sizes of the compounds ranged from 24 to 55 nm. Changes in crystal size were caused by stresses in the structure. Unit cell parameters varied according to the type of dope. This change in the unit cell parameters was derived from the ionic radius diameters of the dope types. As the average ion radius of the doped type increased, the unit cell parameter increased. Thus, the Ce^{+4} ionic radius value was 0.97 Å for VIII coordination, and for the other types: Sm^{3+} (1.079 Å), Gd^{3+} (1.053 Å), Dy^{3+} (1.027 Å), La^{3+}(1.16 Å), Er^{3+}(1.004 Å),Ho^{3+}(1.015Å) , and Y^{3+} (1.019 Å) [18].

Raman spectra were taken at room temperature and provided useful information about the crystal structural defects. The spectra of the samples are given in Fig. 3. Upon examination, the Raman analysis results of pure CeO_2 synthesized via the hydrothermal method show a strong peak at approximately the F_{2g} value at 462 cm^{-1}. With doping, the Ce-O-RE type bonds were formed, and then degradation occurred in the lattice. Oxygen gaps were formed and because any defect in the structure

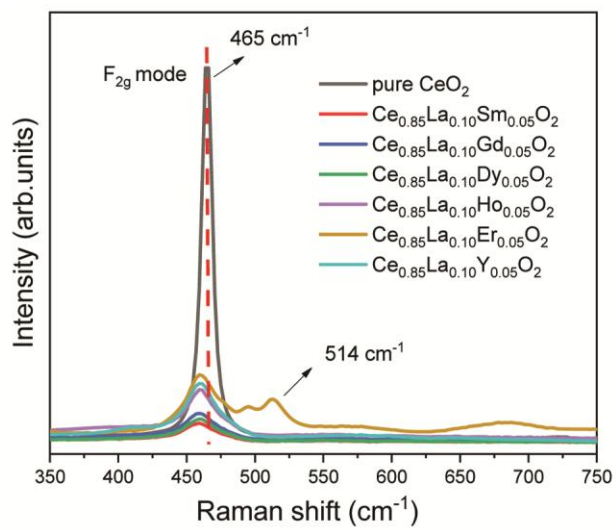

Fig. 3 — Raman spectrum of the compounds CeO_2 and $Ce_{0.85}La_{0.10}M_{0.05}O_2$ (M: Sm^{3+}, Gd^{3+}, Dy^{3+}, Ho^{3+}, Er^{3+}, Y^{3+}).

weakens the electro-phonone interactions, the oxygen became more unstable[19].

Microstructural features of all the synthesized samples were examined via SEM. Figure 4 shows that after the hydrothermal process, the sizes of the samples varied between 100 and 170 nm. As the grain sizes became smaller, the photocatalytic effect increased. The reason for this was that the surface area was increased. Chemical purity and stoichiometric ratios were tested by EDS. When the EDS results (Fig. 5) were examined, it was observed that the stoichiometric ratios determined before the process had been preserved.

Photocatalytic degradation behaviors were examined for all the obtained compounds. The degradation rate behavior of each sample is seen in the graphs in Fig. 6. The degradation graph of the non-photocatalyst solution under a xenon lamp is given. When compared with the graphs for the solutions with photocatalyst particles, it was observed

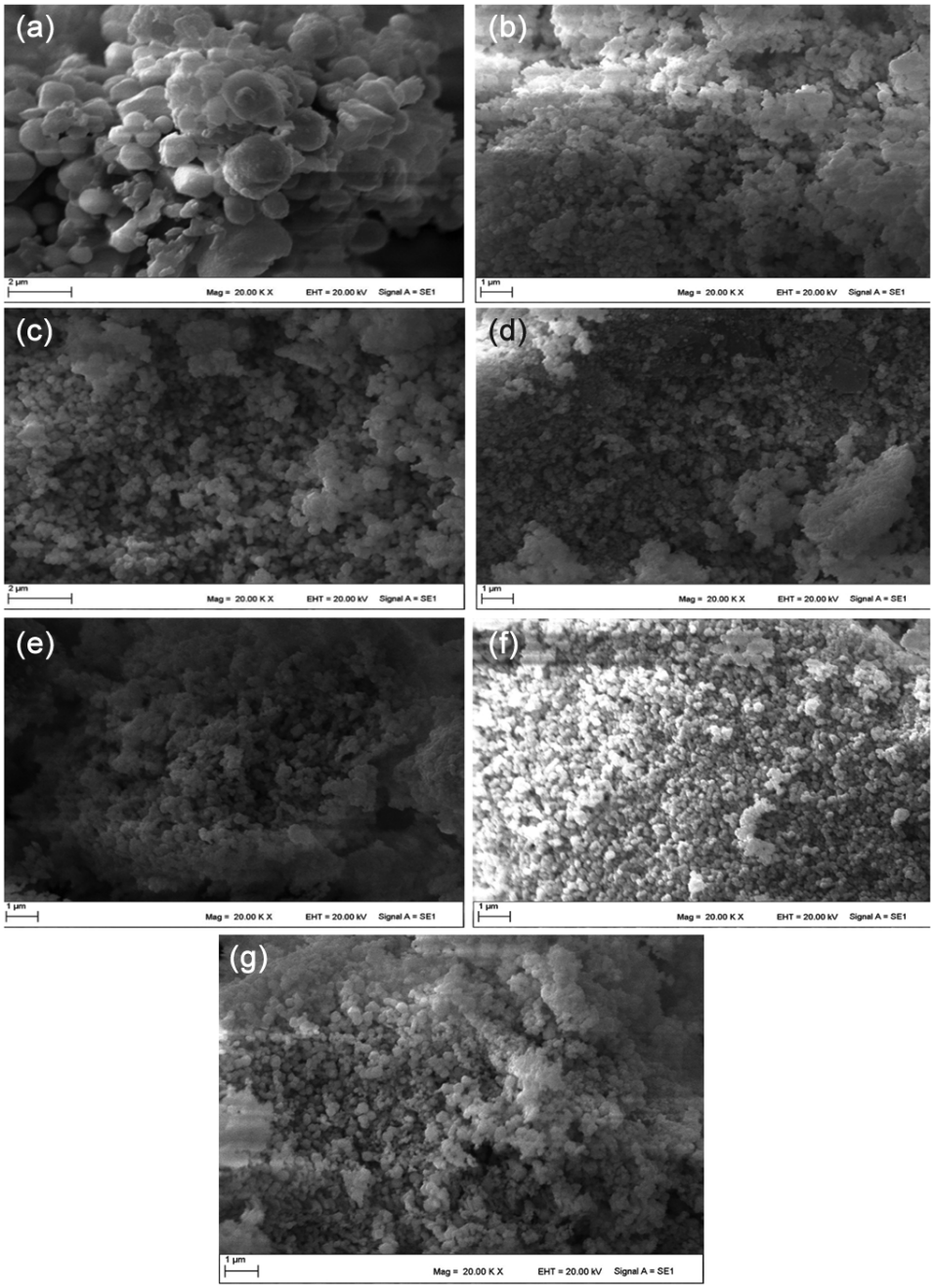

Fig. 4 — SEM images of pure CeO_2 and doped CeO_2 samples: (a) pure CeO_2, (b) La, Sm co-doped CeO_2, (c) La,Gd co-doped CeO_2, (d) La, Dy co- doped CeO_2, (e) La,Ho co-doped CeO_2, (f) La,Er co-doped CeO_2, and (g) La,Yco-doped CeO_2.

that the catalyst particles increased degradation (Fig. 6).

The degradation efficiency (DE) was calculated using Equation (1).

$$DE = \left(1 - \frac{C_t}{C_0}\right) x\ 100 \quad ...(1)$$

In the photocatalysis activity of CeO_2, the band gap and the ability to absorb and release oxygen ions in the crystal structure are important. Indeed, CeO_2 has an optical band gap of 3.2 eV, which strictly limits the application of pure CeO_2 in the ultraviolet (UV) region[20]. To reduce the band gap, rare earths have been doped to the CeO_2. With doping, both Ce^{4+} reduction was inhibited, and oxygen gaps were created for photocatalysis (Fig. 2).

During photocatalysis, methylene blue in the liquid phase is absorbed on the catalyst compound. The catalyst exposed to the light source that

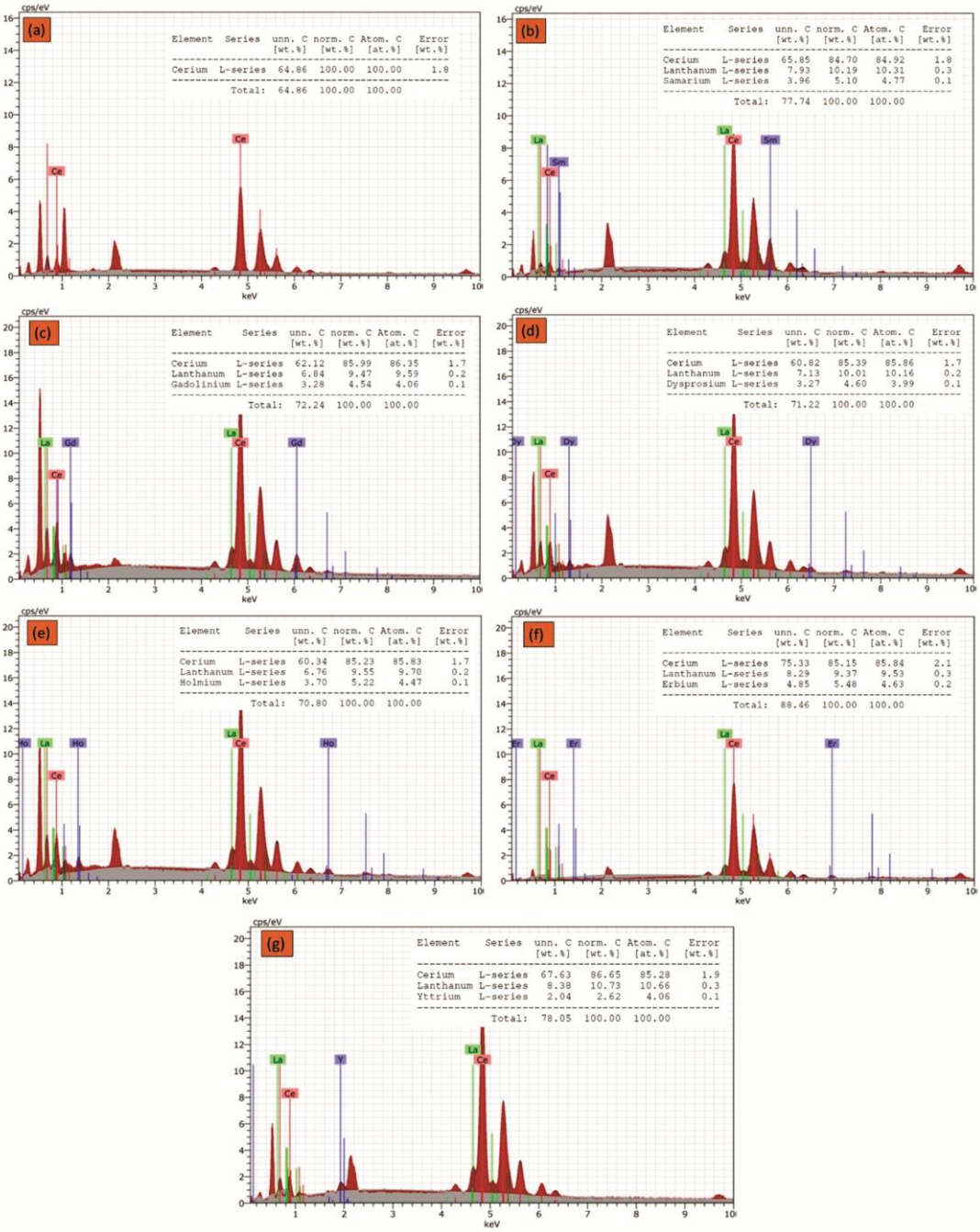

Fig. 5 — EDX images of pure CeO_2 and doped CeO_2 samples: ((a) pure CeO_2, (b) La, Sm co-doped CeO_2, (c) La,Gd co-doped CeO_2, (d) La, Dy co- doped CeO_2, (e) La,Ho co-doped CeO_2, (f) La,Er co-doped CeO_2, and (g) La,Yco-doped CeO_2.

photooxidation in the valence band and photoreduction occurs in the conductor band. The mechanism that occurs with adsorption can be summarized as follows and Fig. 7:

$$\text{Catalyst} + \text{Energy } (h\nu) \longrightarrow \text{Catalyst } (e^- + h^+)$$
$$H_2O + h^+ \longrightarrow OH^{\cdot}\ (\text{radical}) + H^+$$
$$O_2 + e^- \longrightarrow O_2^-\ (\text{superoxide radical})$$
$$O_2^- + H^+ \longrightarrow H_2O$$

The mechanisms indicate that the O_2^- formation and movement were significant. The small diameters of average ions settling in the CeO_2 crystal structure blocked the oxygen ion gaps and prevented movement. Increasing the ion radius of the doping species facilitated electron-ion movement and finally, photocatalytic activity was increased[21].

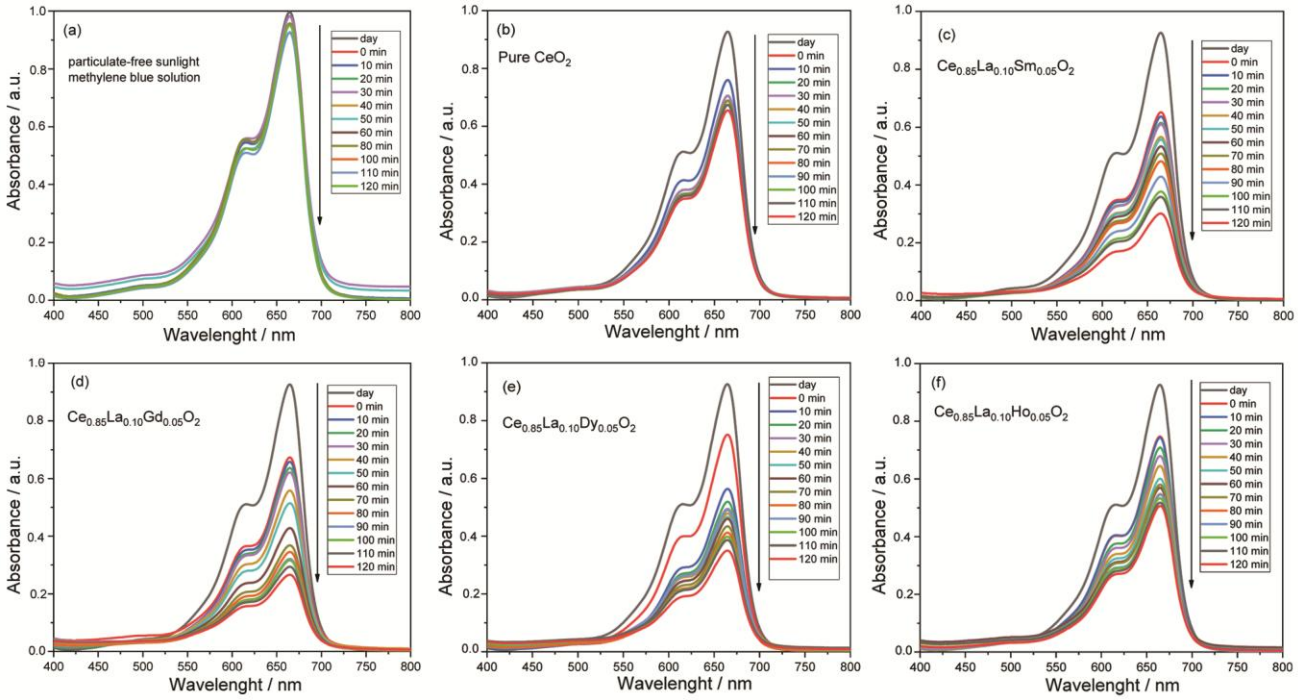

Fig. 6 — Absorption spectra for photocatalytic degradation of MB with catalysts for different time intervals. (a) Simulated sunlight, (b) pure CeO_2, (c)La, Sm co-doped CeO_2, (d) La, Gd co-doped CeO_2, (e) La, Dy co-doped CeO_2, (f) La, Ho co-doped CeO_2, (g) La, Er co-doped CeO_2, and (h) La, Y co-doped CeO_2.

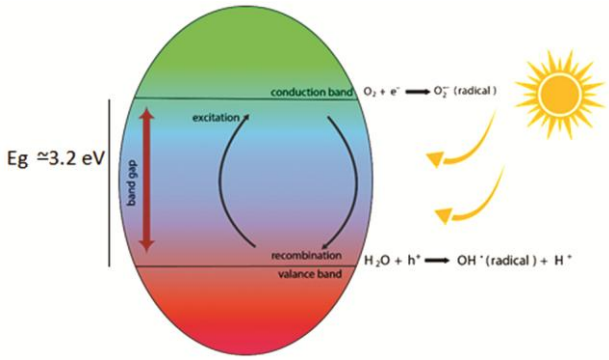

Fig. 7 — Basic mechanism of photodegradation for CeO_2.

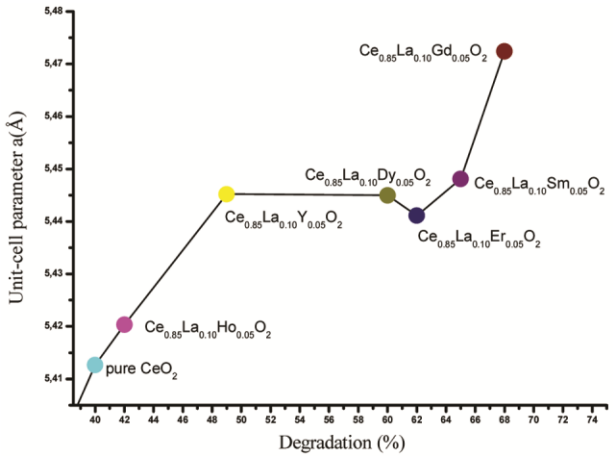

Fig. 8 — Unit cell / degradation change plot.

As seen in the graph of the degradation given in Fig. 8, there is a linear relationship between the degradation and the unit cell parameter. The average radius value of dope types is greater than Ce^{4+}. This situation caused the lattice expansion[16]. Lattice expansion facilitates the movement of the oxygen ion generated during the adsorption of the organic pollutant on the catalysis surface. The exication / recombination event that occurs between the valence band and the conductive band accelerates[22].

Photocatalytic activity is based mainly on the semiconducting nature of a heterogeneous catalyst having a suitable energy band gap. Semiconductors can act as sensitizers for light-induced redox processes due to their electronic structure characterized by a filled valence band and an empty conduction band. The bandgap of all the prepared samples was investigated via UV–Vis diffuse transmission spectra. Figure 9 shows the permeability spectra of the powder particles. The powder particles were obtained via dialysis of ethylene glycol and the particles size was enough to scatter optical visible light. The optical transmittance decreased sharply when the wavelength reached <450 nm. This strong absorption in the UV wavelength region corresponded

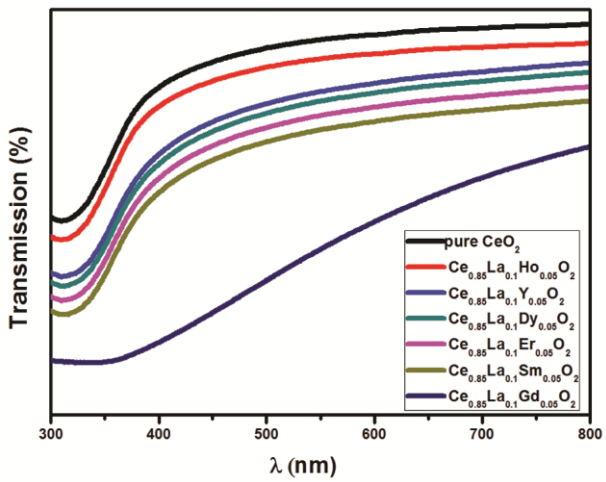

Fig. 9 — Transmission spectra of pure ceria and co-doped ceria.

Table 2 — Photocatalytic Properties of pure CeO_2 and co-doped CeO_2

Samples	Degradation (%)	Band gap (eV)
Particle-free	7	
pure CeO_2	29	3.02
$Ce_{0.85}La_{0.10}Gd_{0.05}O_2$	71	2.02
$Ce_{0.85}La_{0.10}Sm_{0.05}O_2$	67	2.15
$Ce_{0.85}La_{0.10}Er_{0.05}O_2$	65	2.28
$Ce_{0.85}La_{0.10}Dy_{0.05}O_2$	62	2.34
$Ce_{0.85}La_{0.10}Y_{0.05}O_2$	59	2.52
$Ce_{0.85}La_{0.10}Ho_{0.05}O_2$	38	2.71

to the electron transition between the bandgap of the CeO_2. The optical band spacing for the energy of all the prepared samples was calculated using the relationship below as expressed in Equation (2).

$$E_g = \frac{1240}{\lambda(eV)} \quad ...(2)$$

where, E_g represents bandgap energy (eV), and λ the lower cutoff wavelength in nanometers. This may result in a photosynthetically higher photocatalytic performance, with the pure CeO_2 and CeO_2 doped with synthesized powder particles forming more electron-hole pairs under visible light irradiation. The forbidden band ranges of the synthesized types are given in Table 2 using Tauc's method. The study showed that when the rare earth elements were doped, the bandgap decreased from 3.02 to 2.02 eV. According to the results, the $Ce_{0.85}La_{0.10}Gd_{0.05}O_2$ compound had the lowest band range. When compared with the degradation percentages, the results were as expected. The degradation percentage increased in parallel with the band range decreases.

Oxygen voids formed in the crystal lattice increased the percentage of degradation. Degradation percentages of all the types are given in Table 2. The degradation percentage of $Ce_{0.85}La_{0.10}Gd_{0.05}O_2$ solution was calculated as 71% at the end of 120 min and was significantly higher than the others. The chemical stability and crystal structure features of the photocatalyst are among the factors that affected degradation.

4 Conclusions

As a result of this study, seven different elements were successfully added to CeO_2 using the hydrothermal method. The crystal structures obtained at 800 °C sintering temperature were nanosized and exhibited a cubic structure. The particle size was distributed homogeneously. The initially proposed stoichiometric ratios had been preserved. When the particle-free methylene blue dyestuff was compared with the degradation graphs of the solutions, all the obtained compounds were observed to contain additives. According to the photocatalytic results, the highest degradation rate (71%) was determined in the $Ce_{0.85}La_{0.10}Gd_{0.05}O_2$ compound at 2.40 eV in the band ranges. The lowest degradation was observed in the $Ce_{0.85}La_{0.10}Ho_{0.05}O_2$ –doped compound. When the degradation rate, degradation percentage, transmittance, and bandgap results were evaluated together, the results were compatible. According to their effects, the doping types were ranked from high to low as follows: La-Gd, La-Sm, La-Er, La-Dy, La-Y, and La-Ho. The main reason for this originated from the average ion radius factor. The results indicate that La^{3+}-Gd^{3+} is regarded as a better choice as a photocatalyst in the ion doping of CeO_2.

Acknowledgments

This work was supported by Kahramanmaraş Sütçü İmam University and Kahramanmaraş İstiklal University.

References

1 Grabowska E, Appl. Catal. B: Environ, 186 (2016) 97.
2 Maneesha M, Chun D M, App Cat A: Gen, 498 (2015)126.
3 Dong S, Feng J , Fan M, Pi Y, Hu L, Han X & Sun J, RscAdv, 5(2015) 14610.
4 Murakami N, Katayama S, Nakamura M, Tsubota T & Ohno T, J. Phys. Chem, 115 (2011) 419.
5 Gnanasekaran L, Hemamalini R, Saravanan R, Ravichandran K, Gracia F, Agarwal S, Gupta V K, J. Photochem. Photobiol B: Biol, 173 (2017) 43.
6 Xue Y, Zhai Y, Zhou K, Wang L, Tan H, Luan Q & Yao X, Chem. A. European,18 (2012) 11115.
7 Li Z, Niu X, Lin Z, Wang N, Shen H, Liu W &Wang Z J, Alloys Compd, 682 (2016) 647.

8 TanaM, Zhang J, Li Y, Li W. Shen, Catal. Today, 148 (2009) 179.
9 Woan K, Yi-Yang T & Wolfgang S, Nanomedicine, 5 (2010) 233.
10 Abdullah SSBC, Teranishi T, Hayashi H & Kishimoto A, J. Power Sources, 374 (2018) 92.
11 Chin S, Park E, Kim M & Jurng J, Powder Technol, 2011 (2010) 71.
12 Mittal M, Gupta A and Pandey O P, *Solar Energy*, 165 (2018) 206 .
13 Ma R, Zhang S, Wen T, Gu P, Li L, Zhao G, Niu F, Huang Q, Tang Z, Wang X, Catalysis Today, 335 (2019) 20.
14 Yuexiang L, J. Serb. Chem. Soc., 72.4 (2007) 393.
15 Makdee A, Unwiset P, Chanapattharapol KC, Kidkhunthod P, Mater. Chem. Phys., 213 (2018) 431.
16 Peng S, Li Y , Jiang F, Lu G, Li S, Chemical Physics Letters, 398(1-3) (2004) 235.
17 Anirban S & Dutta A, Int. J. Hydrog. Energy, 46 (2020) 25139
18 Shannon RD & Prewitt CD, ActaCryst, 25(1969) 925.
19 Sartoretti E, Novara C, Giorgis F, Piumetti M, Bensaid S, Russo N & Fino D,Sci. Rep, 9 (2019) 1.
20 Hay P J, Martin RL, Uddin J & Scuseria G E, J. Chem. Phys, 125 (2006) 3.
21 Gao XH, Zhou1 B & Yuan R, Environ. Eng. Res, 20 (2015) 329.
22 Bora LV & Maweda RK, Ren. And Sus. Energy Reviews, 76 (2017) 1393.